

INJECTION PHOTODIODES BASED ON METAL OXIDE SEMICONDUCTORS

Vadim Morari¹, Veaceslav Ursaki², Emil Rusu¹, and Ion Tiginyanu²

¹*D. Ghitu Institute of Electronic Engineering and Nanotechnologies, Chisinau, MD-2028
Republic of Moldova*

²*National Center for Materials Study and Testing, Technical University of Moldova, Chisinau,
MD-2004 Republic of Moldova*

E-mail: vvursaki@gmail.com;

(Received August 26, 2020)

DOI: 10.5281/zenodo.4118693

CZU:538.8+539.2+621.382

Abstract

A brief review of our recent research on injection photodiodes based on metal oxide semiconductors deposited onto Si substrates is presented. A series of ZnSnO, NiO, and Zn_{1-x}Mg_xO thin films are prepared by aerosol spray pyrolysis deposition or sol-gel spin coating on Si substrates with a post-deposition thermal treatment in air at a temperature of 500°C. The morphology of films is studied by scanning electron microscopy and atomic force microscopy, while their elemental composition and crystal structure are determined from energy dispersive X-ray (EDAX) and X-ray diffraction (XRD) analysis, respectively. It is shown that the produced *n*-ZnSnO/*p*-Si, *n*-ZnMgO/*p*-Si, and *p*-NiO/*n*-Si heterojunctions operate as injection photodiodes at a forward bias.

Keywords: thin films, aerosol spray pyrolysis, sol-gel spin coating, injection photodiodes.

Rezumat

Este prezentată o analiză succintă a rezultatelor cercetărilor noastre recente obținute pe fotodiode cu injecție în baza materialelor semiconductoare cu oxid de metal depuse pe substraturi de Si. Prin metoda pirolizei cu aerosoli și sol-gel urmată de centrifugare au fost preparate o serie de filme subțiri de ZnSnO, NiO și Zn_{1-x}Mg_xO pe substraturi de Si cu tratament termic post-depunere în aer la temperatura de 500 °C. Morfologia filmelor a fost studiată cu microscopia electronică de scanare și microscopia de forță atomică, iar compoziția chimică și structura cristalină au fost analizate cu dispersia energetică a razelor X (EDAX) și difracția razelor X (XRD), respectiv. S-a arătat că heterojuncțiunile elaborate *n*-ZnSnO/*p*-Si, *n*-ZnMgO/*p*-Si și *p*-NiO/*n*-Si funcționează ca fotodiode cu injecție la polarizare directă.

Cuvinte cheie: Filme subțiri, piroliză cu aerosoli, metoda sol-gel, centrifugare, fotodiode cu injecție.

1. Introduction

Metal semiconductor oxides, especially those in a nanostructured form, have a wide range of applications, in particular, gas sensors, fuel cells, advanced ceramics, chemical sensors, biosensors, batteries, solar cells, pyroelectric, super capacitors, catalysts, and anticorrosion coatings [1–3]. Over the past 5 years, metal oxide semiconductors have been increasingly used in the production of thin-film transistors for flat-panel displays, owing to their high mobility, good transparency, and scalability [4]. The key strategy in these developments relies on the use of heterojunction channels [5].

Among metal semiconductor oxides, ZnO is an important semiconductor and piezoelectric material, which has a high potential for numerous applications, such as phosphors, transparent conducting films, field emission devices, varistors, piezoelectric transducers, resonators, and sensors [6, 7]. The past decade has been marked with an explosion in studying gas sensitive ZnO nanostructures [8–13]. However, despite considerable research efforts and the claimed low-cost, supersensitive, extra-selective, and ultra-rapid parameters, to the best of our knowledge, none of these nanostructures has been significantly implemented into production to show some prospects for the market.

Significant research efforts were also put into study of zinc oxide as a basis for the development of die sensitized solar cells [14]; however, a real progress was achieved only with using ZnO as transparent contacts in various types of solar cells [15, 16].

In addition, there was a significant interest in ZnO-based UV sensors. However, solid solutions are required to control the bandgap of the material and the spectral sensitivity range [17]. The $\text{Zn}_{1-x}\text{Mg}_x\text{O}$ alloy system covers a wide ultraviolet (UV) spectral range between the direct bandgaps of 3.36 eV for ZnO and 7.8 eV for MgO at room temperature [17–21]. However, due to different crystallographic structures of ZnO and MgO, a single-phase material was reliably obtained only for $x = 0\text{--}0.35$ and $0.65\text{--}1$, while a mixed-phase material is formed with intermediate compositions [17, 22].

The $\text{Mg}_{1-x}\text{Ni}_x\text{O}$ alloy system is more promising in this respect, because both NiO and MgO crystallize in a cubic rock-salt structure. It was shown that $\text{Mg}_{1-x}\text{Ni}_x\text{O}$ thin films with high crystalline quality can be grown over the entire composition range [23]; this finding indicates a great flexibility of the $\text{Mg}_{1-x}\text{Ni}_x\text{O}$ system for band gap tuning from 3.7 to 7.8 eV in the deep UV region without phase transition and producing a mixed-phase material [24]. Compositionally and structurally homogeneous epitaxial $\text{Mg}_{1-x}\text{Ni}_x\text{O}$ thin films with $x = 0\text{--}1$, which form a completely miscible solid solution, were grown by pulsed laser deposition on MgO(100) substrates [25].

Zinc stannate (ZTO) was considered as an alternative to binary oxides (ITO, SnO_2 , ZnO) for potential applications in optoelectronic devices and solar energetics due to the low cost, high optical transparency and low electrical resistivity, high electron mobility, and fairly high stability of this material [26]. However, unlike ZnMgO and MgNiO systems, solid solutions can be formed in the ZnSnO system in an amorphous phase only. Concerning the crystalline material, cubic perovskite or LiNbO_3 (LN) type ZnSnO_3 , and cubic inverse spinel Zn_2SnO_4 crystals are formed in this system.

Concerning the conductivity type, the wide-band gap semiconductor NiO (3.7 eV) is one of the few *p*-type transparent conductive oxides exhibiting fairly high electrical properties for application in optoelectronic devices [25]. High-efficiency *p*-NiO/*n*-ZnO [27–29], *p*-NiO/*n*- Ga_2O_3 [30, 31], and *p*-NiO/*n*-Si [32] heterojunction UV photodiodes were reported. On the other hand, photodetectors with *p*-*n* junctions on *n*-type ZnMgO semiconductors deposited onto *p*-type Si substrates were described [19, 21].

The classic *p-n* heterojunction photodiodes operate in the third quadrant of current–voltage characteristics, i.e., at a reverse bias and a negative current. Another type of photodetectors operates as injection photodiodes with internal amplification in the first quadrant, i.e., at a direct bias and a positive current [33, 34]. These types of photodetectors exhibit a high integrated sensitivity. In this paper, we present a brief review of our research on injection photodiodes based on metal oxide semiconductors deposited onto Si substrates.

2. Experimental

Metal oxide films were deposited onto Si substrates by two technological methods. ZnSnO films were deposited by the aerosol spray pyrolysis method. A solution of 0.5 M zinc nitrate [$\text{Zn}(\text{NO}_3)_2$] and 0.5 M tin chloride [SnCl_4] dissolved in ethanol ($\text{C}_2\text{H}_5\text{OH}$) was sprayed onto a *p*-Si substrate using a home-made sprayer with an O_2 gas flow. The substrate was heated in a temperature range of 420–460°C during the deposition. The zinc nitrate and tin chloride solutions with a ratio of 2 : 1 were mixed in an ultrasonic bath at a temperature of 50–60°C for 15 min. A distance of 18 cm between the sprayer and the heated substrate was experimentally chosen in view of obtaining a uniform coverage of the film on the substrate. The solution was injected into the oxygen gas flow by means of a syringe controlled by a computer-operated stepper motor (Jova Solutions TIMS-0201™). The resulting film thickness was determined by the precursor solution injection rate and the deposition process duration. Typically, an injection rate of 0.33 mL/min was used, and the deposition process last for 15 min.

Nickel oxide thin films were prepared by spin coating from sol–gel solutions containing $\text{Ni}(\text{CH}_3\text{CO}_2)_2 \cdot 4 \text{H}_2\text{O}$ nickel(II) acetate tetrahydrate and $\text{Zn}(\text{CH}_3\text{CO}_2)_2$ acetate in respective proportions dissolved in 2-methoxyethanol and diethanolamine (DEA). The solutions were prepared in an ultrasonic bath at a temperature of 50–60°C for 30 min. Spin coating was performed at room temperature on *n*-Si substrates in multiple coating cycles at a rotational speed of 2000 rpm with the rotation taking 20 s followed by drying the coated layer at 150°C for 10 min. After depositing a number of layers, which determine film thickness, the sample was treated at a temperature of 500°C in air for 1 h.

Zinc magnesium oxide thin films were prepared by spin coating from sol–gel solutions containing $\text{Zn}(\text{CH}_3\text{CO}_2)_2$ and $\text{Mg}(\text{CH}_3\text{CO}_2)_2$ acetates in respective proportions dissolved in 20 mL of 2-methoxyethanol + 0.5 mL of DEA. In this study, 0.35 M solutions with an Mg/Zn ratio 0–2/3 were prepared in an ultrasonic bath at a temperature of 50–60°C for 30 min. Spin coating was performed at room temperature on *p*-Si substrates in multiple coating cycles similarly to the above described NiO films.

The morphology and chemical composition microanalysis of the produced films were studied using Zeiss Sigma Hitachi SU 8230 or VEGA TESCAN TS 5130MM scanning electron microscopes equipped with tools for energy dispersive X-ray analysis (EDAX). Atomic force microscopy (AFM) measurements were performed in the tapping mode with a SOLVER Next (NT-MDT) instrument equipped with cone-shaped tips from monocrystalline silicon (tip radius of ~10 nm) on cantilevers with a stiffness of about 17 N/m. The root mean square roughness (RMS) parameters were calculated from the acquired topographic images using the image processing software. X-ray diffraction (XRD) measurements were carried out on a Rigaku SmartLab X-ray diffractometer using CuK_α radiation ($\lambda = 0.15406 \text{ nm}$). The phase was identified by referring to the International Center for Diffraction Data (ICDD PDF-2) database. The current–voltage characteristics and photocurrent of the photodetector structures were measured

with a Keithley 2400 Source Meter Unit (SMU) under illumination with the light selected by optical filters in a wavelength range of 300–400 nm at a power density of 100 mW/cm².

3. Characterization of the Prepared Metal Oxide Films

Figure 1 compares the morphologies of a ZnSnO film deposited by aerosol spray pyrolysis methods and NiO and ZnMgO films prepared by spin coating. The analysis shows that both methods produce thin films with a uniform morphology. However, the roughness of ZnSnO and ZnMgO is higher than that of the NiO films.

These data are confirmed by roughness parameters of the films, which were determined from analysis of AFM images and graphical representations of AFM shown in Fig. 2. The RMS values deduced from the AFM profiles were found to be 13, 10, and 12 nm for ZnSnO, NiO, and ZnMgO films, respectively.

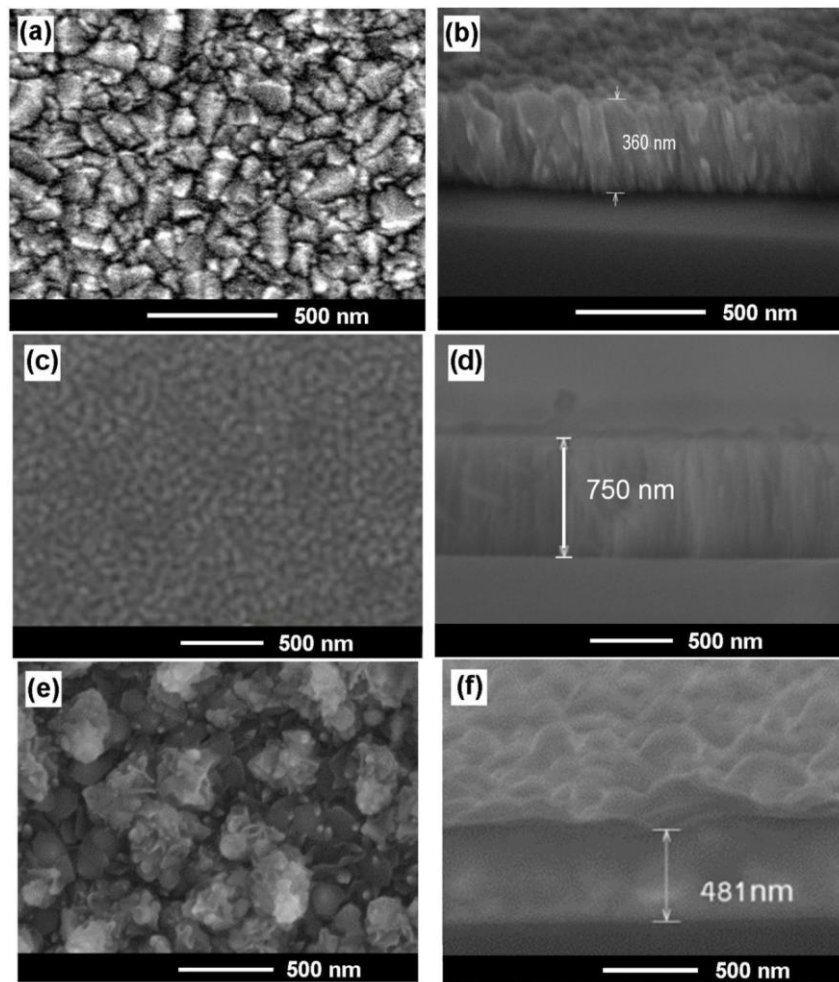


Fig. 1. Frontal (left column) and cross-sectional (right column) SEM images of a ZnSnO film deposited by aerosol spray pyrolysis methods on a *p*-Si substrate (a, b), a NiO film deposited by spin coating on an *n*-Si substrate (c, d), and a ZnMgO film deposited by spin coating on a *p*-Si substrate (e, f).

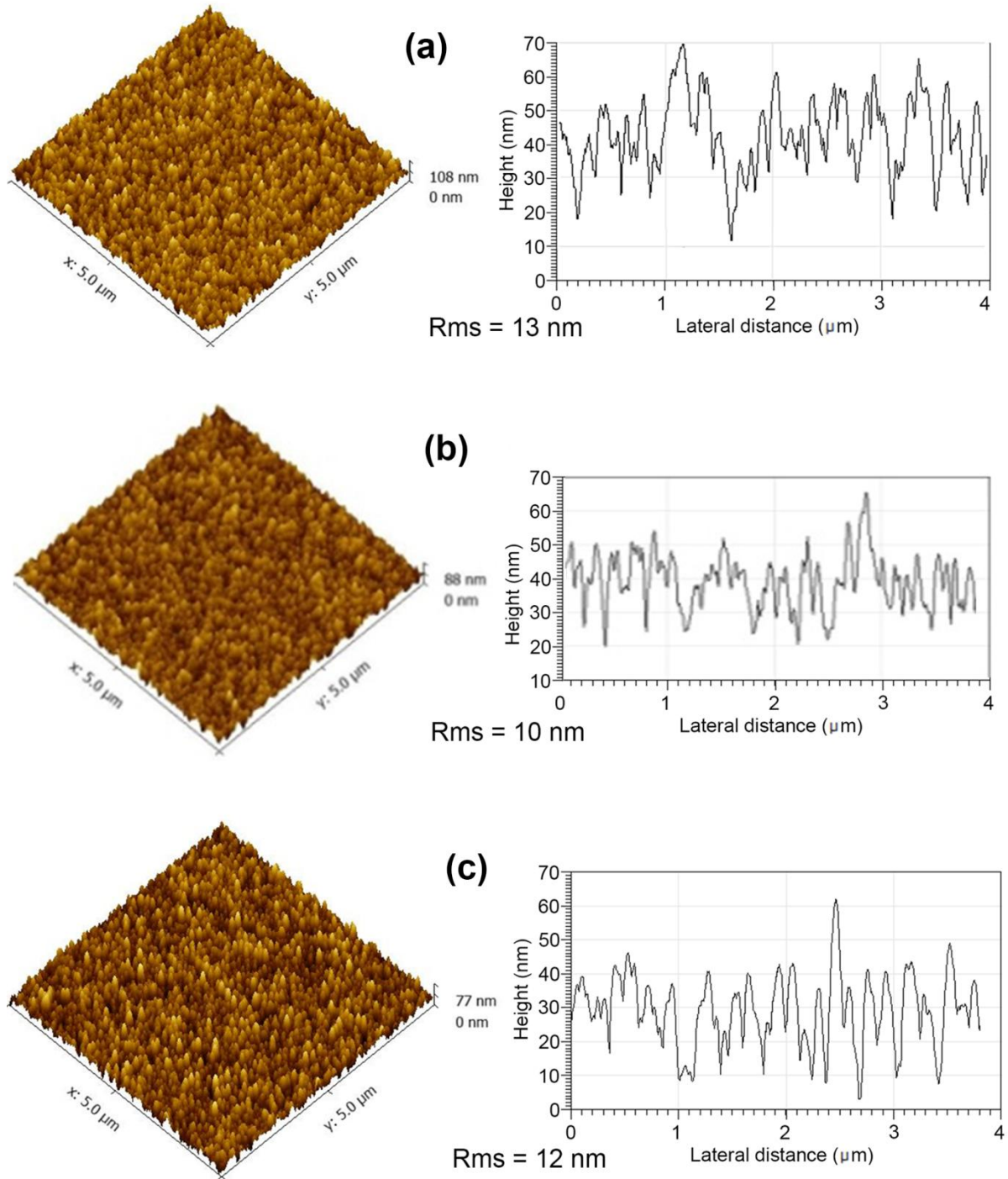


Fig. 2. A $5 \times 5 \mu\text{m}$ 3D AFM image (left column) and graphical representations of the AFM profiles (right column) for a ZnSnO film deposited by aerosol spray pyrolysis methods on a *p*-Si substrate (a), a NiO film deposited by spin coating on an *n*-Si substrate (b), and a ZnMgO film deposited by spin coating on a *p*-Si substrate (c).

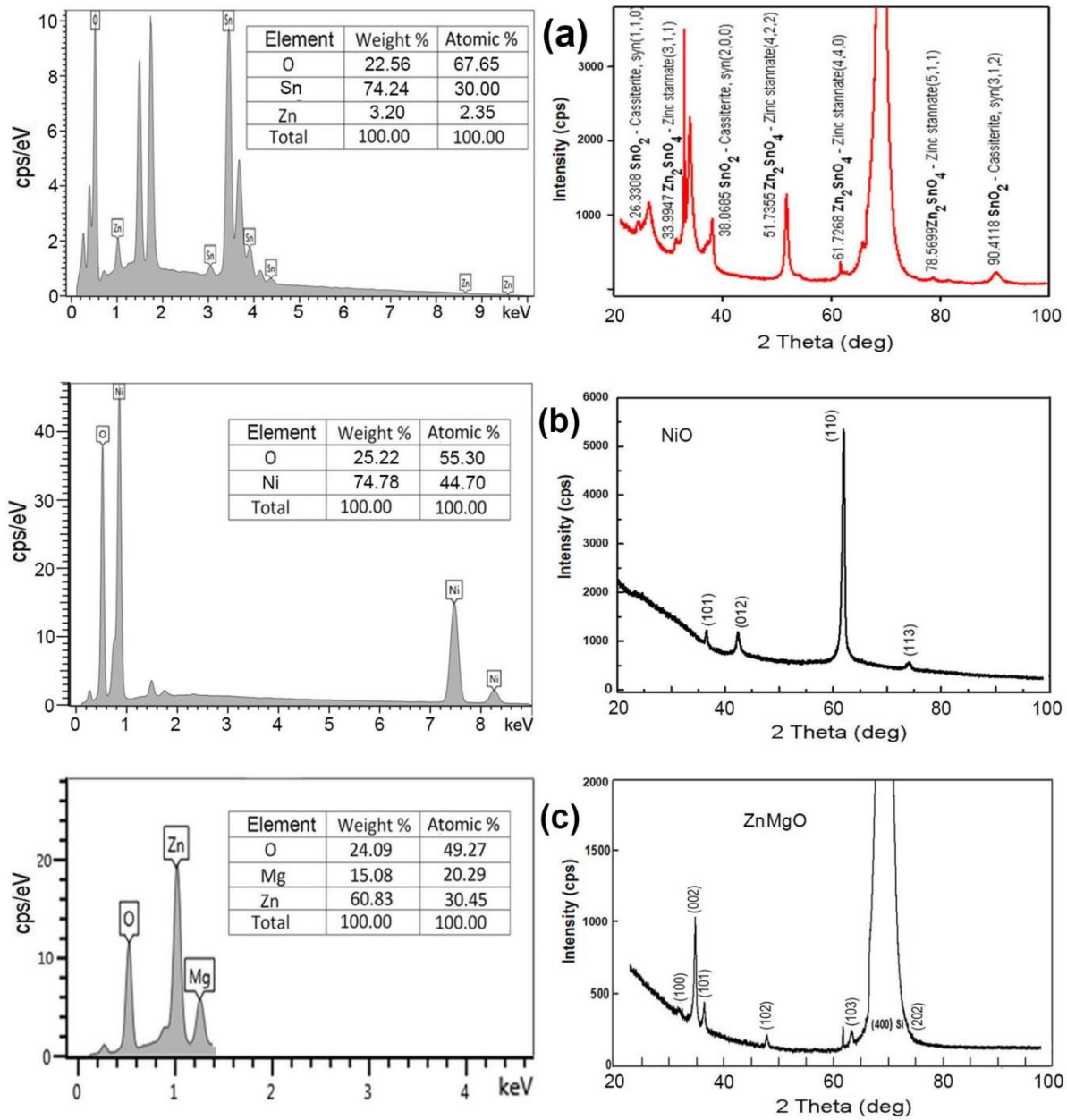


Fig. 3. Elemental composition determined by EDAX analysis (left column) and XRD pattern (right column) of a ZnSnO film deposited by aerosol spray pyrolysis methods on a *p*-Si substrate (a), a NiO film deposited by spin coating on an *n*-Si substrate (b), and a ZnMgO film deposited by spin coating on a *p*-Si substrate (c).

The elemental composition of the prepared films determined by EDAX (Fig. 3, left column) is nearly stoichiometric for the NiO and Zn_{0.6}Mg_{0.4}O films, while the ZnSnO film is composed mostly of SnO₂ crystallites with some inclusions of a ZnSnO phase despite the ratio of 2 : 1 preset in the zinc nitrate and tin chloride precursor solutions. The XRD analysis (Fig. 3, right column) reveals a single-phase rhombohedral structure with space group R-3m (no. 166) for

NiO [35] and a wurtzite phase for the ZnMgO films (PDF card no. 01-078-3032). Concerning the ZnSnO film, the XRD pattern confirms the two-phase composition suggested by the EDAX analysis, with the cassiterite SnO_2 (JCPDS 14-1445) and Zn_2SnO_4 zinc stannate as a second phase [36, 37].

Concerning the optical properties, all the prepared films exhibit a fairly high transparency at a level of 70–80% in the visible and UV spectral range up to 3.6 eV (Fig. 4, left column). The optical bandgap deduced from the Tauc plot (Fig. 4, right column) is 3.40, 3.66, and 3.75 eV for the ZnSnO, NiO, and $\text{Zn}_{0.8}\text{Mg}_{0.2}\text{O}$ films, respectively.

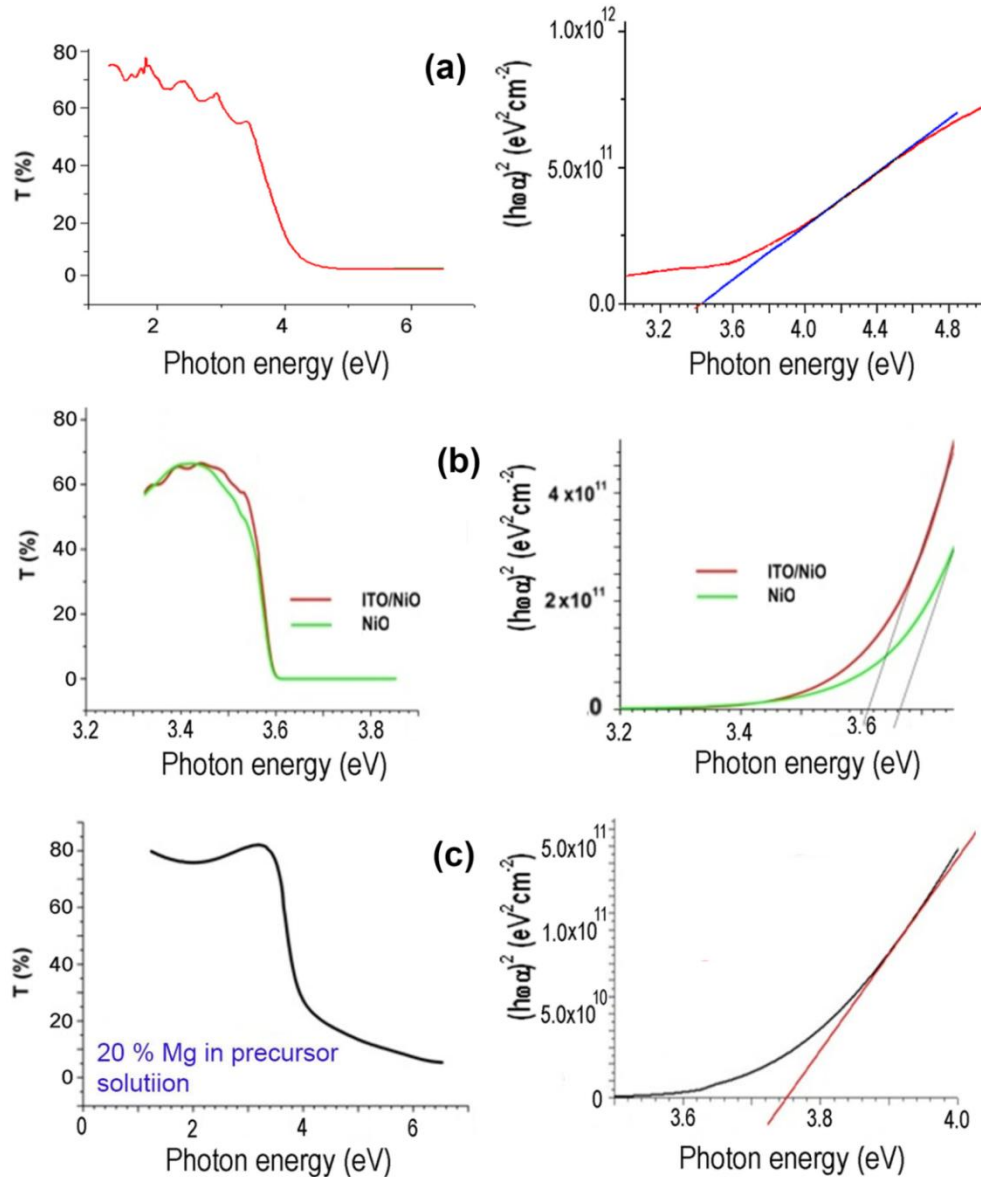


Fig. 4. Optical transmission spectra (left column) and Tauc plot (right column) for a ZnSnO film deposited by aerosol spray pyrolysis methods on a *p*-Si substrate (a), a NiO film deposited by spin coating on an *n*-Si substrate (b), and a ZnMgO film deposited by spin coating on a *p*-Si substrate (c).

4. Characterization of Injection Photodiodes Based on Metal Oxide Semiconductors

The metal oxide films deposited on Si substrates were tested for photodetector applications in a heterostructure design with a metallic contact deposited on the metal oxide film and another contact on the Si substrate. Figures 5 and 6 compare the current–voltage characteristics of metal oxide/Si heterostructures measured in dark and under UV illumination and plotted in linear or double logarithmic coordinates, respectively.

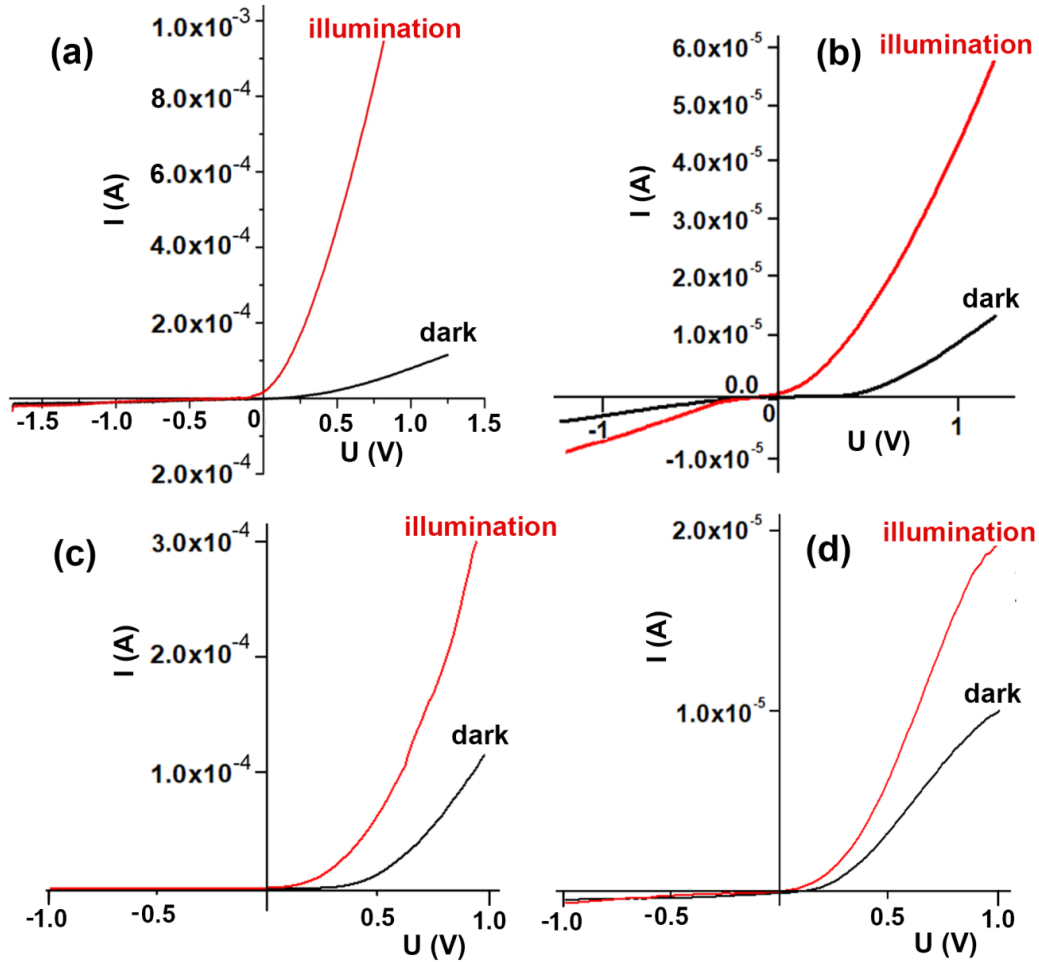


Fig. 5. Current–voltage characteristics at a forward and reverse bias in dark and under UV illumination for a ZnSnO/*p*-Si heterostructure (a), a *p*-NiO/*n*-Si heterostructure (b), a Zn_{0.9}Mg_{0.1}O/*p*-Si heterostructure (c), and a Zn_{0.6}Mg_{0.4}O/*p*-Si heterostructure (d).

All the studied heterostructures exhibit rectifying characteristics. However, in all the cases, the current–voltage characteristic does not fit into the classical formula for a *p*–*n* junction

$$I = I_s \left[\exp\left(\frac{qU}{nkT}\right) - 1 \right].$$

This is especially evident when the current–voltage characteristics are

plotted in semilogarithmic coordinates (not shown here). There should be a straight line for the forward bias in these coordinates; however, it was not observed for any of the studied diodes. Conversely, the characteristics fit into straight lines in double logarithmic coordinates (Fig. 6). Moreover, the studied heterojunctions operate as photodetectors at a forward bias, while a classical $p-n$ junction should function as a photodetector at a reverse bias. The current under a reverse bias under illumination was higher than the dark current by a factor of less than 2 in three of the studied heterostructures. A factor of 2 was obtained only for the p -NiO/ n -Si heterostructure. At the same time, the photocurrent can achieve up to two orders of magnitude at low forward bias values, as observed in Fig. 6.

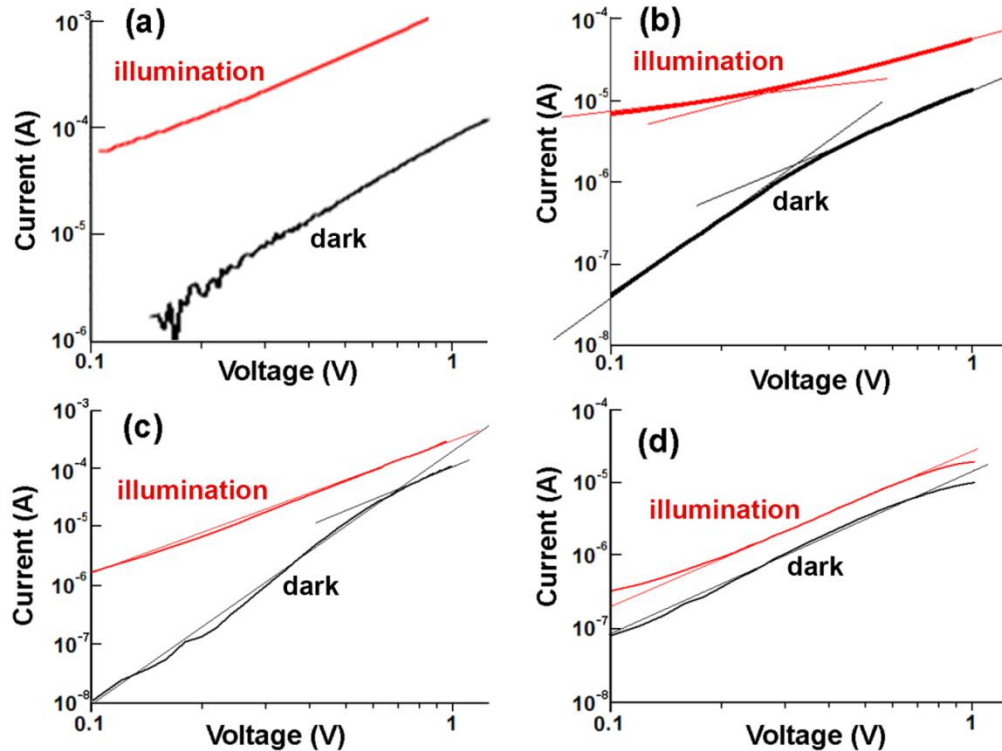


Fig. 6. Current–voltage characteristics at a forward bias in dark and under UV illumination plotted on double logarithmic coordinates for a ZnSnO/ p -Si heterostructure (a), a p -NiO/ n -Si heterostructure (b), a Zn_{0.9}Mg_{0.1}O/ p -Si heterostructure (c), and a Zn_{0.6}Mg_{0.4}O/ p -Si heterostructure (d).

Since the current–voltage characteristics fit into straight lines in the log–log coordinates, they correspond to a power function $I \propto U^n$ according to the Lampert theory [38]. For the n -ZnSnO/ p -Si heterojunction, the n value is about 2 in the dark, which corresponds to the space charge limited (SCL) current injection according to the Mott–Gurney law [39], while the n value decreases under illumination. The n value is also nearly equal to 2 for the p -NiO/ n -Si heterojunction in the dark at biases higher than 0.4 V, while it equals 3 at lower biases. Similarly to the case of n -ZnSnO/ p -Si heterojunction, the n value decreases also for the p -NiO/ n -Si heterojunction under illumination. For the n -Zn_{0.9}Mg_{0.1}O/ p -Si heterojunction, the n value is about 4 in the dark, and it decreases to 2 under illumination. At the same time, the current–voltage

characteristics fit into the MG law both in the dark and under illumination for the $\text{Zn}_{0.6}\text{Mg}_{0.4}\text{O}/p\text{-Si}$ heterojunction (Fig. 6d). These observations suggest that the studied heterojunctions operate as injection photodiodes at a forward bias [33, 34].

5. Conclusions

The obtained results show that the $n\text{-ZnSnO}/p\text{-Si}$, $n\text{-ZnMgO}/p\text{-Si}$, and $p\text{-NiO}/n\text{-Si}$ heterojunctions prepared by spin coating or aerosol spray pyrolysis deposition of metal oxide semiconductor films on Si substrates operate as injection photodiodes at a forward bias. The current–voltage characteristics of these heterojunctions obey power function dependence $I \propto U^n$ according to the Lampert theory. The exponent n value typically decreases under illumination compared with the value in the dark, which equals to 2 in most of the cases corresponding to the space charge limited current injection mechanism according to the Mott–Gurney law. An exception is observed for the $n\text{-Zn}_{0.9}\text{Mg}_{0.1}\text{O}/p\text{-Si}$ heterojunction, for which the exponent value is found to be about 4 in the dark; however, it decreased to 2 under illumination, again obeying the Mott–Gurney law.

Acknowledgments. This work was financially supported by the National Agency for Research and Development of the Republic of Moldova under grant no. 19.80013.50.07.02A/BL and by the Horizon-2020 research and innovation programme of the European Union (grant no. 810652, NanoMedTwin project). The authors also thank Dr. N. Curmei for assistance in preparation of ZnSnO samples by aerosol spray pyrolysis and PhD student A. Pantazi for assistance in AFM and XRD analysis.

References

- [1] S. R. V. Siva Prasanna, K. Balaji, S. Pandey, and S. Rana, Metal Oxide Based Nanomaterials and Their Polymer Nanocomposites, Chapter 4 in Nanomaterials and Polymer Nanocomposites: Raw Materials to Applications, N. Karak, ed., Elsevier Inc., Amsterdam, 2019, pp.123–144, doi:10.1016/B978-0-12-814615-6.00004-7.
- [2] G. N. Dar, Metal Oxide Nanostructures and Their Applications, PhD Thesis, University of Patras, Greece, 2015, p.173.
- [3] S. A. Corr, Metal Oxide Nanoparticles, in Nanoscience: Nanostructures through Chemistry, vol. 1, P. O'Brien ed., RSC publishing, 2013, pp.180–207, doi:10.1039/9781849734844-00180.
- [4] Y. Li, C. Zhao, D. Zhu, P. Cao, S. Han, Y. Lu, M. Fang, W. Liu, and W. Xu, Nanomaterials 10, 965 (2020) doi:10.3390/nano10050965.
- [5] K. M. Kim, W. H. Jeong, D. L. Kim, Y. S. Rim, Y. Choi, M.-K Ryu, K.-B. Park, and H. J. Kim, IEEE Electron Device Lett. 32, 1242 (2011), doi:10.1109/LED.2011.2160612.
- [6] U. Ozgur, Y.I. Aliliv, C. Liu, A. Teke, M.A. Reshchikov, S. Dogan, V. Avrutin, S.-J. Cho, and M. Morkoc, J. Appl. Phys. 98, 041301 (2005), doi:10.1063/1.1992666.
- [7] C. Jagadish and S. Pearton (eds.), Zinc Oxide Bulk, Thin Films and Nanostructures, Processing, Properties and Applications, Elsevier Science, Amsterdam, 2006.
- [8] S. G. Leonardi, Chemosensors 5, 17 (2017), doi:10.3390/chemosensors5020017.
- [9] A. Mirzaei, S. G. Leonardi, and G. Neri, Ceram. Int. 42, 15119 (2016), doi:10.1016/j.ceramint.2016.06.145.

- [10] L. Zhu and W. Zeng, *Sens. Actuators, A* 267, 242 (2017), doi:10.1016/j.sna.2017.10.021.
- [11] V. S. Bhati, M. Hojamberdiev, and M. Kumar, *Energy Rep.* 6, suppl. 4, 46 (2020), doi:10.1016/j.egy.2019.08.070.
- [12] N. Tiwale, *Mater. Sci. Technol.* 31, 1681 (2015), doi:10.1179/1743284714Y.0000000747.
- [13] X. Zhao, R. Zhou, Q. Hua, L. Dong, R. Yu, and C. Pan, *J. Nanomater.* 2015, 854094 (2015), doi:10.1155/2015/854094.
- [14] N. Nemarian, I. Concina, A. Braga, S. M. Rozati, A. Vomiero, and G. Sberveglieri, *Angew. Chem. Int. Ed.* 50, 12321 (2011), doi:10.1002/anie.201104605.
- [15] K. Ellmer, A. Klein, and B. Rech (eds.), *Transparent Conductive Zinc Oxide: Basics and Applications in Thin Film Solar Cells*, Springer, Berlin, Heidelberg, New York, 2008.
- [16] Y. Liu, Y. Li, and H. Zeng, *J. Nanomater.* 2013, 196521 (2013), doi:10.1155/2013/196521.
- [17] J.-L. Yang, K.-W. Liu, and D.-Z. Shen, *Chin. Phys. B* 26, 047308 (2017), doi:10.1088/1674-1056/26/4/047308.
- [18] C.-Z. Wu, L.-W. Ji, C.-H. Liu, S.-M. Peng, S.-J. Young, K.-T. Lam, and C.-J. Huang, *J. Vac. Sci. Technol. A* 29, 03A118 (2011), doi:10.1116/1.3575552.
- [19] Y. N. Hou, Z. X. Mei, H. L. Liang, D. Q. Ye, C. Z. Gu, and X. L. Du, *Appl. Phys. Lett.* 102, 153510 (2013), doi:10.1063/1.4802486.
- [20] J.-S. Shiau, S. Brahma, C.-P. Liu, and J.-L. Huang, *Thin Solid Films* 620, 170 (2016), doi:10.1016/j.tsf.2016.09.037.
- [21] S. S. Maity, P. P. Sahu, and C. T. Bhunia, *IEEE Sens. J.* 18, 6569 (2018), doi:10.1109/JSEN.2018.2849089.
- [22] D. Thapa, J. Huso, H. Che, M. Huso, M. Morrison, D. Gutierrez, M. Grant Norton, and L. Bergman, *Appl. Phys. Lett.* 102, 191902 (2013), doi:10.1063/1.4805005.
- [23] J. W. Mares, R. C. Boutwell, M. Wei, A. Scheurer, and W. V. Schoenfeld, *Appl. Phys. Lett.* 97, 161113 (2010), doi:10.1063/1.3503634.
- [24] D. M. Roessler and W. C. Walker, *Phys. Rev.* 159, 733 (1967), doi:10.1103/PhysRev.159.733.
- [25] C. A. Niedermeier, M. Rasander, S. Rhode, V. Kachkanov, B. Zou, N. Alford, and M. A. Moram, *Sci. Rep.* 6, 31230 (2016), doi:10.1038/srep31230.
- [26] S. Sun and S. Liang, *Mater. Chem. A* 5, 20534 (2017), doi:10.1039/C7TA06221D.
- [27] S.-Y. Tsai, M.-H. Hon, and Y.-M. Lu, *Solid-State Electron.* 63, 37 (2011), doi:10.1016/j.sse.2011.04.019.
- [28] N. Park, K. Sun, Z. Sun, Y. Jing, and D. Wang, *J. Mater. Chem. C* 1, 7333 (2013), doi:10.1039/C3TC31444H.
- [29] M. Patel and J. Kim, *J. Alloys Compd.* 729, 796 (2017), doi:10.1016/j.jallcom.2017.09.158.
- [30] P. Schlupp, D. Splith, H. von Wenckstern, and M. Grundmann, *Phys. Status Solidi A* 216, 1800729 (2019), doi:10.1002/pssa.201800729.
- [31] K.-H. Li, N. Alfaraj, C. H. Kang, L. Braic, M. N. Hedhili, Z. Guo, T. K. Ng, and B. S. Ooi, *ACS Appl. Mater. Interfaces* 11, 35095 (2019), doi:10.1021/acsami.9b10626.
- [32] Y. Zhang, T. Ji, W. Zhang, G. Guan, Q. Ren, K. Xu, X. Huang, R. Zou, and J. Hu, *J. Mater. Chem. C* 5, 12520 (2017), doi:10.1039/c7tc04565d.
- [33] Sh. A. Mirsagatov, A. Yu. Leiderman, and O. K. Ataboev, *Phys. Solid. State* 55, 1635 (2013), doi:10.1134/S1063783413080192.
- [34] Sh. A. Mirsagatov and I. B. Sapayev, *Semiconductors* 48, 1363 (2014), doi:10.1134/S1063782614100212.
- [35] E. Konyshva, E. Suard, and J.T.S. Irvine, *Chem. Mater.* 21, 5307 (2009), doi:10.1021/cm902443n.

- [36] J. E. Jeronsia, A. Joseph, M. M. Jaculine, and S. J. Das, *J. Taibah Univ. Sci.* 10, 601 (2016), doi:10.1016/j.jtusci.2015.12.003.
- [37] S. Dinesh, S. Barathan, V. K. Premkumar, G. Sivakumar, and N. Anandan, *J. Mater. Sci: Mater. Electron.* 27, 9668 (2016), doi:10.1007/s10854-016-5027-y.
- [38] M. A. Lampert, *Rep. Prog. Phys.* 27, 329 (1964), doi:10.1088/0034-4885/27/1/307.
- [39] N. F. Mott and R. W. Gurney, *Electronic Processes in Ionic Crystals*, 2nd ed., Oxford Clarendon Press, 1948.